CHAPTER- IV

DYNAMICAL CONDUCTIVITY OF SYSTEM WITH TWO LAYERS OF CHARGE CARRIERS PER UNIT CELL

Longitudinal and transverse macroscopic as well as microscopic dynamical conductivity are computed for a system having two layers of charge carriers per unit cell, which involve both intralayer and interlayer interactions. It is found that dynamical conductivity of system with two layers per unit cell is not a simple sum of dynamical conductivities of two layers in a unit cell. However, interlayer interactions do not contribute significantly to the dynamical conductivity for $\mathbf{q}$ and q_z tending to zero. The charge carrier in first and second layer of a unit cell interact with each other and their interaction causes a change in the peak position and peak height in macroscopic as well as microscopic conductivities The macroscopic conductivity of doping superlattice is found to be smaller than double heterostructure when frequency is much larger or much smaller as compared with single particle excitation frequency. The difference in conductivity of doping superlattice and of double heterostructure over different wave vector and frequency regimes is caused by the change in Coulomb interaction. The effect of interlayer interaction is maximum when separation between two layers in a unit cell is half of the width of unit cell It is found that the difference in dielectric background of electron and hole layer significantly affect the macroscopic conductivity There exists several transverse electric modes for a single value of wave vector We have computed two adjoining lowest band of transverse electric modes. The frequency range in which transverse modes exist is well separated from that in which plasmons exist. Similar to the case of plasmons, one of the two adjoining transverse electric band is narrow and other one is broad. However, unlike the case of plasmons, frequency of none of transverse electric modes goes to zero as wave vector tends to zero and broad band lies below the narrow band.

4.1 Introduction

The system with two layers of charge carriers per unit cell can be of two types (i) a double heterostructure (DHS) (ii) superlattice having two layers of charge carriers (SL2) per unit cell. The DHS consists of only two layers of charge carriers, whereas SL2 is a periodic

structure along the direction of growth which consists of two layers of charge carriers per unit cell of length, d. For $d \to \infty$, SL2 reduces to DHS. Two layers per unit cell can be of electrons or of holes or one layer of electrons and other of holes. Therefore, both unipolar conduction due to electrons (holes) and bipolar conduction due to electrons as well as holes take place in the system having two layers of charge carriers per unit cell.

SL2 with one electron layer and one hole layer in a unit cell is either a DSSL or a CSSL2. The DSSL consists of one-dimensional periodic sequence of two-layer alternate doping, which is embedded alternatively, in a homogeneous dielectric host medium. The separation of the electron (hole) into narrow layer causes splitting of conduction and valance bands into Q2D subbands, whose spacing can be tailored by choosing approximate design parameters. Therefore, a quantum phenomenon can be observed very well in a DSSL.

The CSSL2 consists of 1D periodic array of electron and hole layers embedded into dielectric medium where background of electrons and holes are different. InAs/GaSb is a good example of CSSL2, where electrons are contained in a InAs layer and holes are contained in a GaSb layer. The calculated subband structure shows a strong dependence on the period of the superlattice. The energy gap decreases with increasing d and the semiconductor to semimetal transition, which results in electron transfer from the GaSb layer to the InAs layer, when the InAs quantum well thickness reaches a threshold.

SL2 with both layers in a unit cell are of electrons (holes) is a CSSL1. GaAs/ $Al_XGa_{1-X}As$ superlattice structure is a good example of CSSL1, consisting of alternate layers of GaAs and $Al_XGa_{1-X}As$. A SL2 of GaAs/$Al_XGa_{1-X}As$ can be fabricated in two ways: (i) All GaAs layers have identical width while two successive $Al_XGa_{1-X}As$ layers are of different widths. The two $Al_XGa_{1-X}As$ layers, of unequal widths, sandwich a GaAs layer and both belong to the same unit cell of superlattice structure. (ii) All $Al_XGa_{1-X}As$ layers are of identical width, whereas two successive layers of GaAs, which sandwich a $Al_XGa_{1-X}As$ are of different widths and the number of electrons per unit area is different in two successive GaAs layers in a unit cell.

Extensive investigations have been carried out on the electronic properties of DSSL [1-4]. Detailed theoretical study on the electronic and optical properties of a DSSL shows that, in spite of impurity scattering, well behaved plasmon modes could be observed in DSSL because of tunable carrier density and nearly perfect separation of electrons and holes [5]. It

has been demonstrated that, for 2DEG consisting of random impurity potential, plasma oscillations can be observed for reasonably high values of carrier density for restricted values of wave vector [6]. Metzner et.al [7] investigated intralayer relaxation process and pair recombination in doped n-i-p-i structure after a pulse excitation. They demonstrated that the introduction of a fixed donor-acceptor pair distance leads to drastic changes in recombination kinetics. In the last few years, a number of experiments on GaAs DSSL have been carried out to demonstrate the tunability of bipolar conductivity [8], absorption coefficient [9-11], photoluminescence [12] and electroluminescence [13] and subband spacing by an externally applied voltage or by optical excitation [14-15].

The optical absorption coefficient, in heavy doped n and p type GaAs is evaluated and is found that absorption coefficient is very sensitive to the density of electron states and band gap shrinkage [11,14,15]. Experimental measurements on photocurrent and photoluminescence of these materials have revealed that the optical properties of DSSL are quite different from those of all bulk materials and ordinary superlattice [16-17]. The optical detection of vertical transport [18-19] offers the possibility of measuring the diffraction properties of carrier motion along the growth axis without modifying the electronic states of the structure.

Collective excitation spectrum of CSSL2 has been studied for non-tunneling [20-24] as well as for tunneling case [25-28]. Dispersion curves for surface and bulk plasmons [21-25], surface polaritons [29-30] as well as surface phonons [31-34] have been studied theoretically as well experimentally for CSSL2. It has been shown that collective excitations are very sensitive to the variation of thickness of the layer and this effect is clearly reflected in electron energy loss spectra. Phonons in GaAs/AlAs CSSL2 have been observed directly in Raman scattering experiments and it is found that optical phonons are completely confined within either GaAs or AlAs layers [35]. Sawaki et al. [36] calculated the scattering rates in GaAs/AlAs CSSL2, assuming that confined electrons interact only with LO phonons confined to the same layer and having vanishing displacements at the interfaces. The results showed that the polaron damping rate decreases with the narrowing of the well layer.

Non-linear high electric field hot carrier transport in CSSL2 employing a force and energy balance approach has been investigated taking into account of both intralayer and interlayer carrier-carrier interaction between like carriers as well as interactions between electrons and holes [37-39]. Carrier-phonon and carrier-impurity scattering interactions are

also included [40]. Linear high field transport is also examined with the determination of memory function contribution due to dynamically screened electron-hole scattering.

It has been demonstrated that large absorption coefficients are obtained in the infrared region when InAs well thickness (d_1) and $Ga_{1-x}InSb$ barrier thickness (d_2) are of the order of d_1=39 Å and d_2=25 Å [41] These small values of d_1 and d_2 increase the interface roughness scattering and the mobility, μ for that mechanism scale can be approximated as $\mu_{IR} \propto d_2^6$ [42]. A comprehensive single particle formalism for both in plane and growth direction free carrier transport in CSSL2 has been worked out [43]. It is found that, in the limit of large barrier to well thickness ratios, the formalism reproduces expressions for Q2D, while in the opposite limit of thin barriers, transport in CSSL2 becomes analogous to that in a 3D semiconductor with an anisotropic effective mass. While the CSSL2 mobility usually falls between the two limits, it frequently differs from both [44]. The approximate electron concentration and mobility parallel to the plane wire derived for Hall measurements at 4.2 K in low magnetic field. The electron mobility for InAs quantum wells of thickness of 150-200 Å. ranges between 1.5 and 2 $\times 10^5$ cm^2/V sec at 4.2 K [45]. Transport measurements in CSSL2 conducted by several groups showed negative differential conductance [46-47]. Magneto transport measurements on a series of n type InAs-$Ga_{1-x}In_xSb$ superlattices with thin wells and barriers led to the observation of diagonal conductivity (Shubnikov de Hass oscillations) as well as Hall conductivity (oscillations in σ_{xy}) [48].

Existing theoretical investigations on collective excitations and dynamical conductivity of DSSL, CSSL2 and DHS, which are reviewed above have following shortcomings:

(1) Most of the theoretical studies have been performed for small wave vector and they are not valid for all values of wave vector and frequency

(2) The dynamical response of DSSL, CSSL2 and DHS involve both intralayer as well as interlayer interactions because of two layers of charge carriers per unit cell in these systems. Contribution from interlayer interactions to dynamical macroscopic and microscopic conductivity become significant at large value of wave vector, which has not been properly dealt in existing studies of dynamical conductivity and collective excitations.

(3) How does the difference in structure of DSSL, CSSL2 and DHS affect the dynamical conductivity and collective excitations has not been properly addressed in existing work reported above.

In this chapter, we report our theoretical study on macroscopic and microscopic dynamical conductivity for SL2 (DSSL and CSSL2) and DHS using formalism reported in chapter-II. The GaAs DSSL can be modelled as periodic sequence of electron and hole layers embedded alternately in a polarizable host media of dielectric function $\varepsilon(\omega)$ and of a unit cell (which comprises one electron and one hole layer) of length d along z-axis. The electrons and holes in the GaAs DSSL are mainly confined to their respective layers and their motion along z-axis can be described with the use of wave functions and energy eigen values of harmonic oscillator. Our model CSSL2 structure consists of alternate layers of electrons and holes along z-axis, where background dielectric media of electrons is different than that for holes. We take d_1 as the thickness of an electron layer and d_2 as the thickness of a hole layer. The length of the unit cell along z-axis, which is the sum of d_1 and d_2 is taken to be d. An example of CSSL2 offers a two-component plasma in an inhomogeneous background. The lattice which consists of electrons is different from that containing holes, in a unit cell. The electron and holes plasmas interact with each other in addition to their interaction with lattice vibrations of InAs and GaSb Our calculation incorporates intralayer and interlayer interactions and are valid for all values of wave vector and frequencies. The calculation of the dynamical conductivity of SL2 and DHS are reported in sec.4.2 while the result and discussion of them are discussed in sec.4.3. This chapter is summarized in sec.4 4.

4.2 Calculation of dynamical conductivity

As is reported in chapter II, general equations of dynamical macroscopic and microscopic conductivities are given by the relations,

$$\sigma^{L/T}(\mathbf{r},\mathbf{r}',\omega) = (\gamma - i\omega/4\pi) \int V(\mathbf{r},\mathbf{r}'') \, \alpha^{L/T}(\mathbf{r}'',\mathbf{r}',\omega) \, d\mathbf{r}'', \qquad (4.1)$$

$$\tilde{\sigma}^{L}(\mathbf{r},\mathbf{r}',\omega)=\sigma^{L}(\mathbf{r},\mathbf{r}',\omega)-\iint\tilde{\sigma}^{L}(\mathbf{r},\mathbf{r}_1,\omega)V(\mathbf{r}_1,\mathbf{r}_2)\alpha^{L}(\mathbf{r}_2,\mathbf{r}',\omega)d^3\mathbf{r}_1 d^3\mathbf{r}_2 \qquad (4.2)$$

and

$$\tilde{\sigma}^T(\mathbf{r},\mathbf{r}',\omega)=\sigma^T(\mathbf{r},\mathbf{r}',\omega)+(i\omega/c^2)\iint\sigma^T(\mathbf{r},\mathbf{r}_1,\omega)G(\mathbf{r}_1,\mathbf{r}_2,\omega)\tilde{\sigma}^T(\mathbf{r}_2,\mathbf{r}',\omega)\, d^3\mathbf{r}_1\, d^3\mathbf{r}_2, \qquad (4.3)$$

where

$$V(\mathbf{r},\mathbf{r}') = e^2/|\mathbf{r}-\mathbf{r}'| \qquad (4.4a)$$

and

$$G(\mathbf{r},\mathbf{r}',\omega)=\exp[(i\omega/c)|\mathbf{r}-\mathbf{r}'|]/|\mathbf{r}-\mathbf{r}'|\,. \qquad (4.4b)$$

The $\alpha^{L/T}(\mathbf{r},\mathbf{r}',\omega)$ is defined by Eq.(2.21). After taking the Fourier transformation in x-y co-ordinates, Eqs.(4.1) and (4.3) can be transformed to

$$\sigma^{L/T}(\mathbf{q},z,z',\omega)= (\gamma-i\omega/4\pi)\int V(\mathbf{q},z,z'')\,\alpha^{L/T}(\mathbf{q},z'',z',\omega)\, dz'', \qquad (4.5)$$

$$\tilde{\sigma}^L(\mathbf{q},z,z',\omega)=\sigma^L(\mathbf{q},z,z',\omega)-\iint\tilde{\sigma}^L(\mathbf{q},z,z_1,\omega)V(\mathbf{q},z_1,z_2)\alpha^L(\mathbf{q},z_2,z',\omega)\, dz_1 dz_2 \qquad (4.6)$$

and

$$\tilde{\sigma}^T(\mathbf{q},z,z',\omega) = \sigma^T(\mathbf{q},z,z',\omega) + (i\omega/c^2)\iint\sigma^L(\mathbf{q},z,z_1,\omega)\,G(\mathbf{q},z_1,z_2,\omega)\,\tilde{\sigma}^T(\mathbf{q},z_2,z',\omega)\, dz_1\, dz_2, \qquad (4.7)$$

where $V(\mathbf{q},z_1,z_2)$ and $G(\mathbf{q},z_1.z_2.\omega)$ are defined by the Eqs.(3.4a) and (3 4b). We further consider the case of superlattice where electrons and holes are mainly confined to their respective layers (non-tunnelling superlattices). Confinement of motion gives rise to discrete energy levels along z-axis. The z-motion is described with the use of envelope functions has been reported in Ref.[50] and [51]. We solve Eqs (4.5) and (4 7) by assigning the width d_1 and d_2 to electron and hole layer, respectively. The length of unit cell, $d \geq d_1+d_2$. the ordinate of lth unit cell can be defined as

$$z = ld + R_j + t \quad \text{with } -d_j/2 \leq t \leq d_j/2. \qquad (4.8)$$

Here. R_j is the distance of the jth layer of lth unit cell from the bottom of cell. j varies over the unit cell and can take two values (1 and 2). Equations (4.5) and (4.7) with the use of Eq.(4.8) are transformed into following integral equations.

$$\sigma_{ij}^{L/T}(\mathbf{q},l,l',t,t',\omega)=(\gamma-i\omega/4\pi)\sum_{l''}\int V_{ij}(\mathbf{q},l,l'',t,t'')\alpha_{jj}^{L/T}(\mathbf{q},l'',l',t'',t',\omega)dt'', \tag{4.9}$$

$$\tilde{\sigma}_{ij}^{L}(\mathbf{q},l,l't,t',\omega)=\sigma_{ij}^{L}(\mathbf{q},l,l',t,t',\omega)\delta_{ij} - \sum_{l_1}\iint\tilde{\sigma}_{ij'}^{L}(\mathbf{q},l,l_1,t,t_1,\omega)V_{j'j}(\mathbf{q},l_1,t_1,l_2,t_2)$$

$$\alpha_{jj}^{L}(\mathbf{q},t_2,t',\omega)\,dt_1\,dt_2 \tag{4.10}$$

and

$$\tilde{\sigma}_{ij}^{T}(\mathbf{q},l,l't,t',\omega) = \sigma_{ij}^{T}(\mathbf{q},l,l',t,t',\omega)\delta_{ij} + (i\omega/c^2)\sum_{l_1,l_2}\iint dt_1 dt_2\,\tilde{\sigma}_{ij'}^{T}(\mathbf{q},l,l_1,t,t_1,\omega)$$

$$G_{j'j}(\mathbf{q},l_1,t_1,l_2,t_2,\omega)\sigma_{jj}^{T}(\mathbf{q},l_2,l',t_2,t',\omega) \tag{4.11}$$

with

$$V_{ij}(\mathbf{q},l,l',t,t')=(2\pi e^2/\mathbf{q})\exp[-\mathbf{q}|(l-l')d+R_{ij}+(t-t')|] \tag{4.12a}$$

and

$$G_{ij}(\mathbf{q},l,l',t,t',\omega)=(2\pi/\mathbf{p})\exp[-\mathbf{p}|(l-l')d+R_{ij}+(t-t')|], \tag{4.12b}$$

where δ_{ij} is Kronecker delta function and $R_{ij} = R_i-R_j$, which is the distance between ith and jth layer of a unit cell As i and j can take two values, σ_{ij} ($\tilde{\sigma}_{ij}$) is a 2×2 matrix in i and j. Further, each element of σ_{ij} ($\tilde{\sigma}_{ij}$) can form a matrix in terms of subband index However, in this chapter, we confine to intrasubband transitions in ground subband. Equations (4 9) to (4.12) are further simplified with the use of discrete Fourier transform with respect to l and l' in a manner similar to that described in chapter III. After algebraic simplifications, we obtain

$$\sigma_{ij}^{L/T}(\mathbf{q},q_z,\omega) = (\gamma_i-i\omega/4\pi)V_{ij}(\mathbf{q},q_z)\alpha_{jj}^{L/T}(\mathbf{q},\omega) - (i\omega/4\pi)\,\delta_{ij}\,[\varepsilon_{ij}(\omega)-1], \tag{4.13}$$

$$\tilde{\sigma}_{ij}^{L}(\mathbf{q},q_z,\omega) = \tilde{\varepsilon}_{ij}^{-1}(\mathbf{q},q_z,\omega)\,\sigma_{ij}^{L}(\mathbf{q},q_z,\omega) \tag{4.14}$$

and

$$\tilde{\sigma}_{ij}^{T}(\mathbf{q},q_z,\omega) = \tilde{F}_{ij}^{-1}(\mathbf{q},q_z,\omega)\,\sigma_{ij}^{T}(\mathbf{q},q_z,\omega), \tag{4.15}$$

where $\bar{\varepsilon}^{-1}_{ij}(\mathbf{q},q_z,\omega)$ and $\bar{F}^{-1}_{ij}(\mathbf{q},q_z,\omega)$ are the inverse of longitudinal dielectric response function, $\varepsilon_{ij}(\mathbf{q},q_z,\omega)$ and transverse response function, $F_{ij}(\mathbf{q},q_z,\omega)$, respectively which are defined as

$$\varepsilon_{ij}(\mathbf{q},q_z,\omega) = \delta_{ij}\,\varepsilon_{ij}(\omega) + V_{ij}(\mathbf{q},q_z)\,\alpha^{L/T}_{jj}(\mathbf{q},\omega) \qquad (4.16)$$

and

$$F_{ij}(\mathbf{q},q_z,\omega) = \delta_{ij} + [(\gamma_j - i\omega)/c^2]\,G_{ij}(\mathbf{q},q_z,\omega)\,\sigma^{T}_{jj}(\mathbf{q},q_z,\omega). \qquad (4.17)$$

γ_j is the inverse of transport relaxation of a charge carrier in jth layer of a unit cell. The $\varepsilon_{jj}(\omega)$ is background dielectric function which involve lattice vibrations. A simple form of $\varepsilon_{jj}(\omega)$ is given as

$$\varepsilon_{jj}(\omega) = \varepsilon_{\infty j}\,[\omega(\omega+i\gamma_{ph})-\omega_{Lj}])\,/\,[\omega(\omega+i\gamma_{ph})-\omega_{Tj}]. \qquad (4.18)$$

The γ_{ph} is the phenomenological damping parameter for phonons. The ω_{Lj} and ω_{Tj} are the frequencies of longitudinal and transverse optical phonon mode, respectively in jth layer of a unit cell. $\varepsilon_{\infty j}$ is high frequency dielectric constant of jth layer. For homogeneous background (same background for charge carriers in two layers in a unit cell), $\varepsilon_{11}(\omega)= \varepsilon_{22}(\omega)$, whereas for the case of charge in two layers, within a unit cell, having different background $\varepsilon_{11}(\omega)\neq\varepsilon_{22}(\omega)$. For this case of energy involved in electronic transitions is much larger than ω_{Lj} (ω_{Tj}). $\varepsilon_{jj}(\omega) \sim \varepsilon_{\infty j}$. The $V_{ij}(\mathbf{q},q_z) = (2\pi e^2/\mathbf{q})\,U_{ij}(\mathbf{q},q_z)$, where $U_{ij}(\mathbf{q},q_z)$ is structure factor which is defined as

$$U_{ij}(\mathbf{q},q_z)= [H_{ij}(\mathbf{q})-C_{ij}(\mathbf{q})]\,\delta_{ij}+C_{ij}(\mathbf{q})\,W_{ij}(\mathbf{q},q_z), \qquad (4.19)$$

where

$$W_{ij}(\mathbf{q},q_z)=\{[(\exp(-\mathbf{q}|R_{ij}|)\exp(iq_zd)\,/\,(\exp(q_zd)-\exp(i\mathbf{q}d))] + [(\exp(\mathbf{q}|R_{ij}|)\exp(-\mathbf{q}d)/(\exp(-q_zd)-\exp(-i\mathbf{q}d))]\}. \qquad (4.20)$$

$W_{ij}(\mathbf{q},q_z) \equiv W_{ji}(\mathbf{q},-q_z) \equiv W^{*}_{ji}(\mathbf{q},q_z)$ and $|R_{ii}|=|R_{jj}|=0$ and $|R_{ij}|=d_S$. The d_S is separation between two layers of charge carriers in a unit cell. Similarly, $G_{ij}(\mathbf{q},q_z,\omega) = (2\pi/\mathbf{p})\,U_{ij}(\mathbf{p},q_z)$, where $U_{ij}(\mathbf{p},q_z)$ and $W_{ij}(\mathbf{p},q_z)$ are obtained from Eqs. (4.19) and (4.20) on replacing $\mathbf{q}$ by $\mathbf{p}$. The envelope function along z-direction can be taken as wave function of harmonic oscillator

if the boundaries of layer of charge carriers are diffusive, which is the case of DSSL [49]. For such a superlattice, matrix elements $H_{ii}(\mathbf{q})$ and $C_{ij}(\mathbf{q})$ are given by [49]

$$H_{ii}(\mathbf{q})=\exp(\mathbf{q}^2/\alpha_i^2) - (\sqrt{2}\mathbf{q}/\sqrt{\pi}\,\alpha_i)\exp[-\mathbf{q}^2/2\alpha_i^2] \qquad (4.21)$$

and

$$C_{ij}(\mathbf{q})=\exp\{(\mathbf{q}^2/4)[1/\alpha_i^2+1/\alpha_j^2]\}, \qquad (4.22)$$

where

$$\alpha_j=(4\pi e^2 m_j^* N_{D/A}/\hbar^2\varepsilon_{\infty j})^{1/2}. \qquad (4.23)$$

$N_{D/A}$ is the number of donars or acceptors per unit volume and m_j^* is the effective mass of the charge carrier. When the boundary of layer of charge carriers are sharp (abrupt), infinite potential well wave functions can be used to describe z-motion of charge carrier in a layer [50]. The abrupt boundaries appear in CSSL2 The $H_{ii}(\mathbf{q})$ and $C_{ij}(\mathbf{q})$ with the use of infinite potential well wave function are given as [50]

$$H_{ii}(\mathbf{q}) = [u_i/x+2/u_i] - 32(\pi^2/xu_i)^2[1-\exp(-u_i)] \qquad (4.24)$$

and

$$C_{ij}(\mathbf{q})= g_i(\mathbf{q})\, g_j(-\mathbf{q}), \qquad (4.25)$$

where

$$g_i(\mathbf{q}) = (4\pi^2/xu_i)[1-\exp(-u_i)] \qquad (4.26)$$

with $u_i=qd_i$ and $x=u_i^2+4\pi^2$ and $y=u_i^2$. The effective longitudinal microscopic conductivity, $\tilde{\sigma}_2^L(\mathbf{q},q_Z,\omega)$ and transverse microscopic conductivity $\tilde{\sigma}_2^T(\mathbf{q},q_Z,\omega)$ are now given by

$$\tilde{\sigma}_2^L(\mathbf{q},q_z,\omega)=\tilde{\sigma}_{11}^L(\mathbf{q},q_z,\omega)+\tilde{\sigma}_{12}^L(\mathbf{q},q_z,\omega)+\tilde{\sigma}_{21}^L(\mathbf{q},q_z,\omega)+\tilde{\sigma}_{22}^L(\mathbf{q},q_z,\omega) \quad (4.27)$$

and

$$\tilde{\sigma}_2^T(\mathbf{q},q_z,\omega)=\tilde{\sigma}_{11}^T(\mathbf{q},q_z,\omega)+\tilde{\sigma}_{12}^T(\mathbf{q},q_z,\omega)+\tilde{\sigma}_{21}^T(\mathbf{q},q_z,\omega)+\tilde{\sigma}_{22}^T(\mathbf{q},q_z,\omega). \quad (4.28)$$

Equation (4.14) and (4.15) can be rewritten in the form similar to Eqs.(3.11) and (3.12), respectively. We denote $\tilde{\sigma}_2^L(\mathbf{q},q_Z,\omega)$ and $\tilde{\sigma}_2^T(\mathbf{q},q_Z,\omega)$ as

$$\tilde{\sigma}_2^{L}(\mathbf{q},q_z,\omega)=\sigma_2^{L}(\mathbf{q},q_z,\omega)\,/\,\varepsilon_2(\mathbf{q},q_z,\omega) \tag{4.29}$$

and

$$\tilde{\sigma}_2^{T}(\mathbf{q},q_z,\omega)=\sigma_2^{T}(\mathbf{q},q_z,\omega)\,/\,F_2(\mathbf{q},q_z,\omega), \tag{4.30}$$

where $\sigma_2^{L}(\mathbf{q},q_z,\omega)$ and $\sigma_2^{T}(\mathbf{q},q_z,\omega)$ represents as the macroscopic longitudinal and transverse conductivity, respectively. Similarly, $\varepsilon_2(\mathbf{q},q_z,\omega)$ and $F_2(\mathbf{q},q_z,\omega)$ are response functions for longitudinal and transverse fields, respectively. They are defined as

$$\sigma_2^{L}(\mathbf{q},q_z,\omega)=[1/\sqrt{\varepsilon_{11}(\omega)\varepsilon_{22}(\omega)}]\{\sigma_{11}^{L}(\mathbf{q},q_z,\omega)\,[\varepsilon_{22}(\mathbf{q},q_z,\omega)-\varepsilon_{12}(\mathbf{q},q_z,\omega)]+$$

$$\sigma_{22}^{L}(\mathbf{q},q_z,\omega)\,[\varepsilon_{11}(\mathbf{q},q_z,\omega)-\varepsilon_{21}(\mathbf{q},q_z,\omega)]\} \tag{4.31}$$

and

$$\sigma_2^{T}(\mathbf{q},q_z,\omega)=[1/\sqrt{\varepsilon_{11}(\omega)\varepsilon_{22}(\omega)}]\{\sigma_{11}^{T}(\mathbf{q},q_z,\omega)\,[F_{22}(\mathbf{q},q_z,\omega)-F_{12}(\mathbf{q},q_z,\omega)]$$

$$+\sigma_{22}^{T}(\mathbf{q},q_z,\omega)\,[F_{11}(\mathbf{q},q_z,\omega)-F_{21}(\mathbf{q},q_z,\omega)]\}, \tag{4.32}$$

where

$$\varepsilon_2=(1/\sqrt{\varepsilon_{11}\varepsilon_{22}})\begin{vmatrix}\varepsilon_{11} & \varepsilon_{12}\\ \varepsilon_{21} & \varepsilon_{22}\end{vmatrix} \tag{4.33}$$

and

$$F_2=\begin{vmatrix}F_{11} & F_{12}\\ F_{21} & F_{22}\end{vmatrix}. \tag{4.34}$$

The ε_{11} and ε_{22} (F_{11} and F_{22}) involve intralayer interactions, whereas ε_{12} and ε_{21} (F_{12} and F_{21}) are related to interlayer interactions We have noticed that generalised equation for dynamical conductivity given in chapter-II can be used to describe the conductivity of superlattice having more than two layers of charge carriers in a unit cell

4.3 Results and discussion

This section is divided in two parts. The macroscopic conductivity is discussed in first part, whereas second part is devoted to the discussion of microscopic conductivity.

4.31 Macroscopic conductivity

The macroscopic conductivity for longitudinal field is given by $\sigma_2^L(\mathbf{q},q_z,\omega)$, whereas the macroscopic conductivity for transverse field is given be $\sigma_2^T(\mathbf{q},q_z,\omega)$. We first consider the case of homogeneous background $[\varepsilon_{11}(\omega) = \varepsilon_{22}(\omega)]$ and also we ignore the ω-dependence of ε_{11} and ε_{22} (a static background dielectric constant. The $\sigma_2^{L/T}(\mathbf{q},q_z,\omega)$ can be written as sum of two parts

$$\sigma_2^{L/T}(\mathbf{q},q_z,\omega) = \sigma'_{L/T}(\mathbf{q},q_z,\omega) + \sigma''_{L/T}(\mathbf{q},q_z,\omega), \qquad (4.35)$$

where

$$\sigma'_{L/T}(\mathbf{q},q_z,\omega) = \sigma_{11}^{L/T}(\mathbf{q},q_z,\omega) + \sigma_{22}^{L/T}(\mathbf{q},q_z,\omega) \qquad (4.36)$$

and

$$\sigma''_{L/T}(\mathbf{q},q_z,\omega) = \sigma_{11}^{L/T}(\mathbf{q},q_z,\omega)\,\alpha_{22}^{L/T}(\mathbf{q},\omega)\,[V_{22}(\mathbf{q},q_z)-V_{12}(\mathbf{q},q_z)] + \sigma_{22}^{L/T}(\mathbf{q},q_z,\omega)\alpha_{11}^{L/T}(\mathbf{q},\omega)[V_{11}(\mathbf{q},q_z)-V_{21}(\mathbf{q},q_z)]. \qquad (4.37)$$

The $\sigma'_{L/T}(\mathbf{q},q_z,\omega)$ involves intralayer interactions, whereas $\sigma''_{L/T}(\mathbf{q},q_z,\omega)$ consists of interlayer as well as intralayer interactions. This suggests that $\sigma_2^{L/T}(\mathbf{q},q_z,\omega)$ is not the simple sum of macroscopic conductivities of two layers in a unit cell. For $\mathbf{q}\to 0$ and $q_z\to 0$, $V_{11}=V_{21}$ and $V_{22}=V_{12}$, which gives $\sigma''_{L/T}(\mathbf{q},q_z,\omega)=0$. Therefore, only intralayer interactions contribute to the macroscopic longitudinal conductivity for $\mathbf{q}$ and q_z tending to zero When one of the two layers in a unit cell belong to electrons and other belongs to holes, the electronic part of $\sigma_2^L(\mathbf{q},q_z,\omega)$ for both q and q_z tending to zero is given by

$$\sigma_{2e}^L(\omega) = [n_{s1}e^2/m_1(\gamma_1-i\omega)] + [n_{s2}e^2/m_2(\gamma_2-i\omega)], \qquad (4.38)$$

where n_{s1} and n_{s2} are the 2D carrier densities, γ_1 and γ_2 are the damping constants and m_1 and m_2 are the masses of electrons and holes, respectively. Equation (4.38) is classical result

of conductivity of a system consisting of two types of charge carriers. For non-zero value of **q** and q_z, the interlayer interactions contribute significantly to the macroscopic longitudinal or transverse conductivity, $\sigma_{2e}^{L/T}(\mathbf{q},q_z,\omega)$, obtained using Eq.(4.35), significantly differs from $\sigma_L(\omega)$ even for $qd<<1$ and $q_z d<<1$ when qv_F is not very small as compared with $|\omega+i\gamma|$.

In order to see the variation of $\sigma_2^L(\mathbf{q},q_z,\omega)$ with **q** , we consider the case of $q_z\rightarrow 0$ and $\omega=0$. For small **q**, $\sigma'_{L/T}(\mathbf{q})$ can be given by

$$\sigma'_{L/T}(\mathbf{q}) = \sigma_d + \beta' q^2, \tag{4.39}$$

where

$$\sigma_d = n_{s1}e^2/m_1\gamma_1 + n_{s2}e^2/m_2\gamma_2, \tag{4.40}$$

$$\beta' = \beta_1 n_{s1}e^2/m_1\gamma_1 + \beta_2 n_{s2}e^2/m_2\gamma_2, \tag{4.41a}$$

$$\beta_1 = d^2/12 - 3\hbar^2 k_{F1}/4m_1\gamma_1, \tag{4.41b}$$

and

$$\beta_2 = d^2/12 - 3\hbar^2 k_{F2}/4m_2\gamma_2. \tag{4.41c}$$

β' in Eq.(4.39) can be negative ($\beta'<0$) or positive ($\beta'>0$) depending on the value of n_{s1}, n_{s2}, γ_1, γ_2, d, m_1 and m_2. Independent of value of β', $\sigma''_L(\mathbf{q})$ always increases with **q** in small **q**-range and is independent of n_{s1}, n_{s2}, γ_1, γ_2 or d. This suggests that $\sigma_2^L(\mathbf{q})$ can be greater than or smaller than σ_d depending on β'.

For the case of CSSL2, where $\varepsilon_{11}(\omega)\neq\varepsilon_{22}(\omega)$, the electronic part of $\sigma_2^L(\mathbf{q},q_z,\omega)$ for both **q** and q_z tending to zero is given by

$$\sigma_{2e}^L(\omega) = n_{s1}e^2\sqrt{\varepsilon_{22}}/[m_1(\gamma_1-i\omega)\sqrt{\varepsilon_{22}}] + n_{s2}e^2\sqrt{\varepsilon_{11}}/[m_2(\gamma_2-i\omega)\sqrt{\varepsilon_{22}}], \tag{4.42}$$

which is different from $\sigma_{2e}^L(\omega)$ given by Eq (4.37) Equation (4.42) shows that unlike the inhomogeneous background case, electronic part of σ^L is affected by lattice vibrations of two material in unit cell. Also, conductivity of electrons (holes) is affected by their background of both electrons and holes. Their relative contribution are determined by $\varepsilon_{11}/\varepsilon_{22}$.

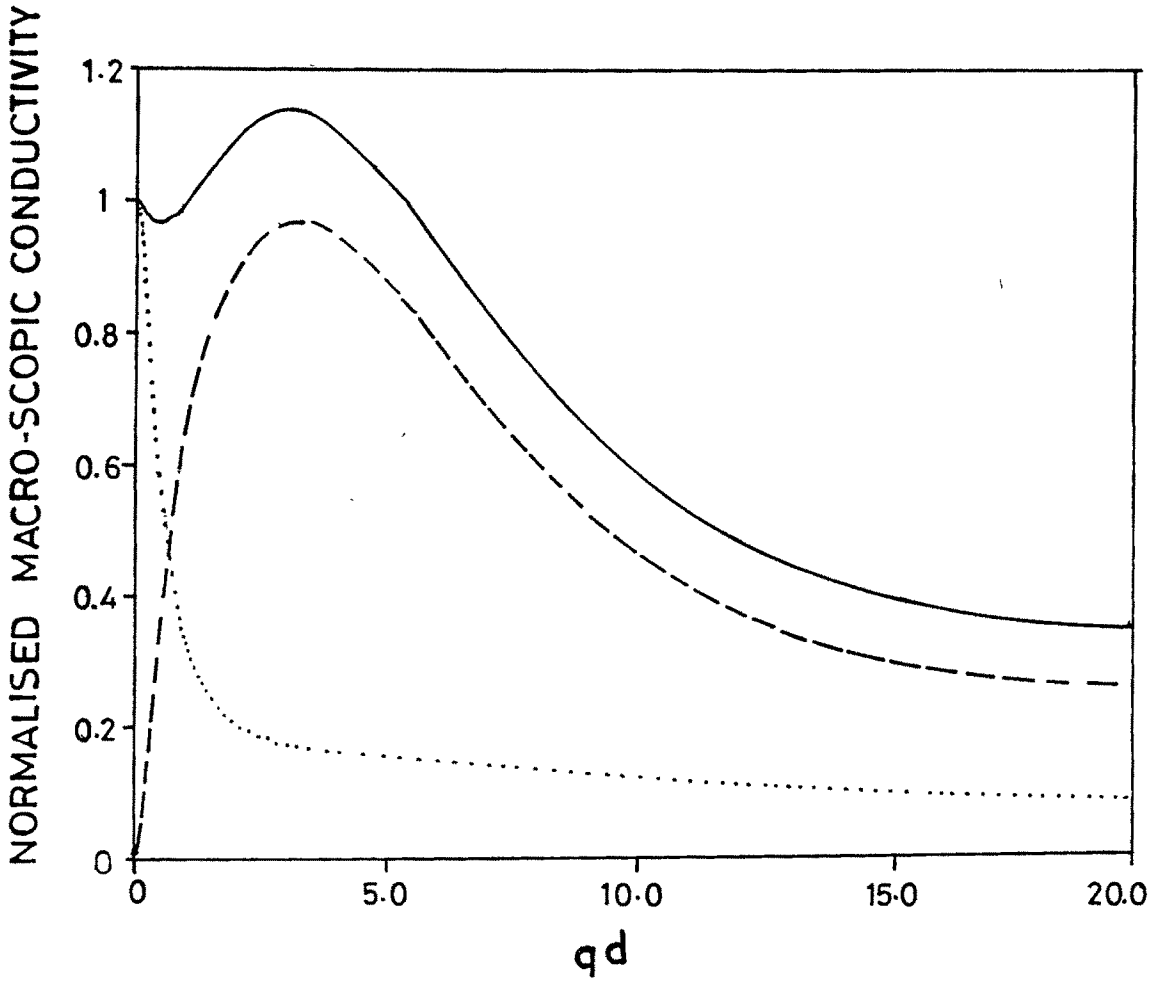

Fig. 4.1 A plot of $\sigma_{2e}^{L}(\mathbf{q})/\sigma_d$ (solid line), $\sigma_{2e}'(\mathbf{q})/\sigma_d$ (dot-dot curve) and $\sigma_{2e}''(\mathbf{q})/\sigma_d$ (dashed curve) versus $\mathbf{q}d$ at $\omega=0$ and $q_z d=0$ for GaAs DSSL.

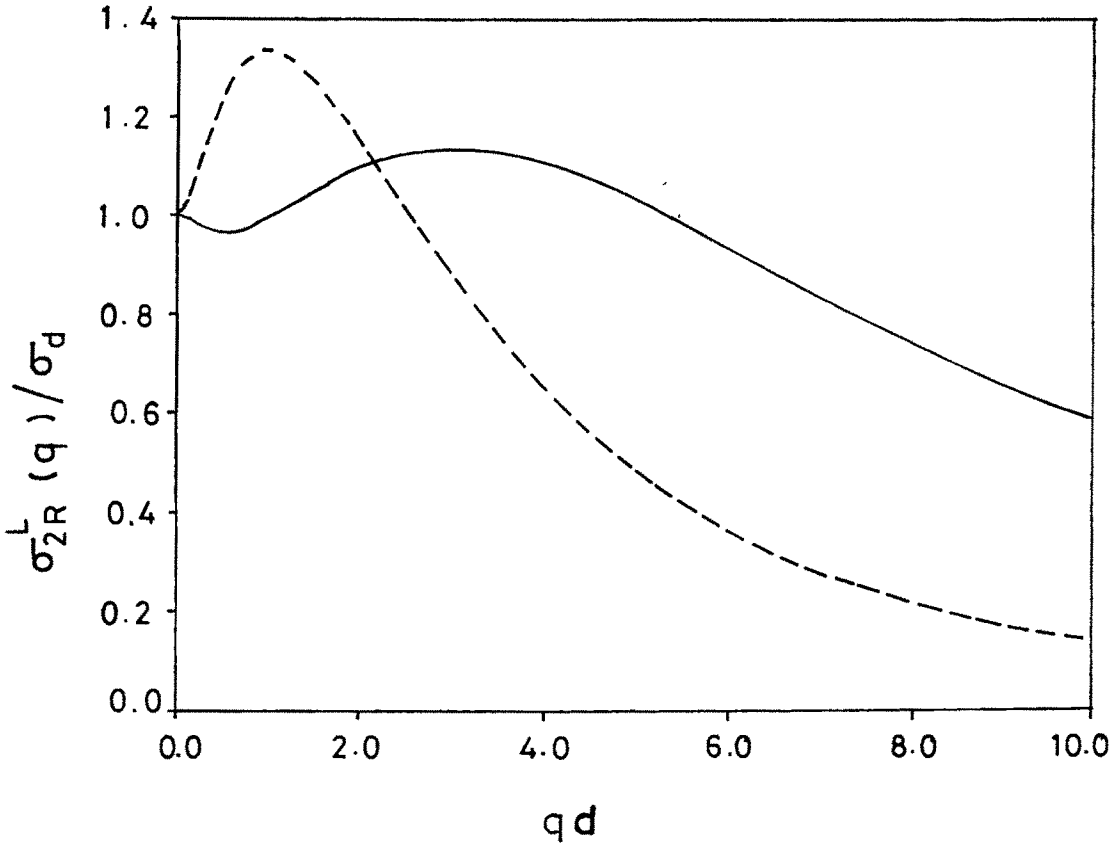

Fig. 4.2(a) The $\sigma^L_{2R}(\mathbf{q})/\sigma_d$ for DHS (dashed curve) and DSSL (solid line curve) is plotted as a function of **q**d for ω=0 and $q_z d$=0.

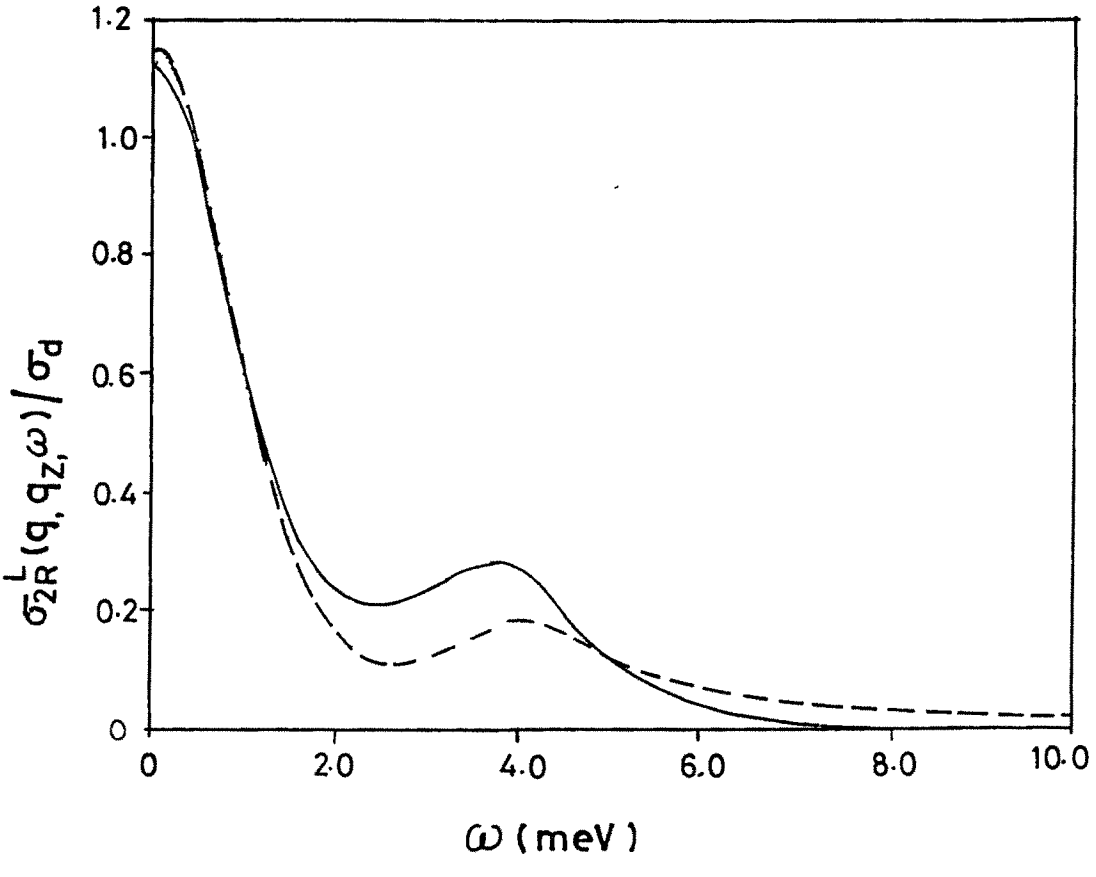

Fig. 4.2(b) A plot of $\sigma^{L}_{2R}(\mathbf{q}, q_z, \omega)/\sigma_d$ versus ω at $q_z d$=1.0 and $\mathbf{q}d$=2.0. Dashed curves and solid line curve represent DHS and DSSL, respectively.

Computed $\sigma^{L}_{2R}(\mathbf{q},q_z,\omega)$, real part of $\sigma^{L}_{2}(\mathbf{q},q_z,\omega)$ as a function of ω shows two peaks whose positions are approximated by $\omega \sim qv_{F1}$ and $\omega \sim qv_{F2}$. The important point to be seen is how interlayer interaction affects peak positions and peak heights on inclusion of second layer in the unit cell. The v_{F1} and v_{F2} are determined by n_{s1}, n_{s2}, m_1 and m_2, respectively. Therefore, the shape of peaks and separation between them is governed by the carrier densities and masses of the charge carriers in two layers of a unit cell. The broad feature of two peaks in σ^{L}_{2}, which correspond to single excitation peak are similar to that of single particle excitation peak observed in σ^{L} reported in chapter III. Like $\sigma^{T}_{R}(\mathbf{q},q_z,\omega)$, $\sigma^{T}_{2R}(\mathbf{q},q_z,\omega)$ has no peak and it decreases monotonically and reduces to a very small value for large ω. Unlike the case of $\sigma^{L}_{2R}(\mathbf{q},q_z,\omega)$, interlayer interactions do not significantly contribute to $\sigma^{T}_{2R}(\mathbf{q},q_z,\omega)$ and for $\omega \rightarrow 0$, contribution from interaction goes to zero.

We have computed $\sigma^{L}_{2e}(\mathbf{q})$, electronic part of $\sigma^{L}_{2}(\mathbf{q},q_z,\omega)$ for $\omega=0$ and $q_zd=0$ for GaAs DSSL. For computation we used following values of parameters: $m_1=0.07\ m_e$, $m_2=0.7\ m_e$, $n_{s1}=n_{s2}=10^{12}\ cm^{-2}$, $\varepsilon_\infty=10.9$, $d_1=600$ Å, $d_2=500$ Å, d_s (width of undoped layer)$=100$ Å, $\omega_{L0}=36.57$ meV, $\omega_{T0}=33.845$ meV and $\gamma_1=\gamma_2=1.0$ meV. Our results are plotted in Fig. 4.1. Figure shows that $\sigma'_{2e}(\mathbf{q})$ which involves intralayer interactions has largest value for $\mathbf{q}d \rightarrow 0$, which the $\sigma''_{2e}(\mathbf{q})$ shows maximum value at around $\mathbf{q}d=3.5$ The shape and position of peak in $\sigma''_{2e}(\mathbf{q})$ is determined by m_1, m_2, n_{s1}, n_{s2}, d and d_s. The behaviour of $\sigma^{L}_{2e}(\mathbf{q})$ in small $\mathbf{q}$-range ($\mathbf{q}d \leq 5$) depends on m_1, m_2, n_{s1}, n_{s2}, d and d_s. It is found that when the layer are of same type, $\sigma^{L}_{2e}(\mathbf{q})$ always increases on increasing effective mass of charge carrier.

Behaviour of $\sigma^{L}_{2R}(\mathbf{q},q_z,\omega)$ with $\mathbf{q}d$ at non-zero ω values is found similar to of $\sigma^{L}_{2R}(\mathbf{q},q_z,\omega)$ with ω at fixed $\mathbf{q}d$. This suggests that the behaviour of $\sigma^{L}_{2R}(\mathbf{q},q_z,\omega)$ with one out of $\mathbf{q}$, q_z or ω keeping other two quantities fixed is of similar nature. It can therefore, be concluded that $\mathbf{q}$, q_z and ω all are equally important variables in determining macroscopic conductivity of a type-II superlattices. Frequency dependent macroscopic dynamical conductivity should be computed by averaging over $\mathbf{q}$ and q_z but not by taking $\mathbf{q}d \rightarrow 0$ and $q_zd \rightarrow 0$ limit to make a comparison between theory and experiment. It is found that maximum peak height in σ^{L}_{2R} of DSSL is obtained when n_{s1} is close to n_{s2} and d_s is very close to d/2, whereas maximum peak height is obtained when n_{s1} and d_s are not very close to n_{s2} and d/2, respectively.

Our computed $\sigma^{L}_{2R}(\mathbf{q},q_z,\omega)/\sigma_d$ is plotted as function of $\mathbf{q}$ at $q_zd=0$ and $\omega=0$ in Fig. 4.2(a) and as a function of ω at $q_zd=1.0$ and $\mathbf{q}d=2.0$ in Fig 4.2(b) for GaAs DSSL and DHS The DHS consists of one electron layer and one hole layer, whereas DSSL is multilayered

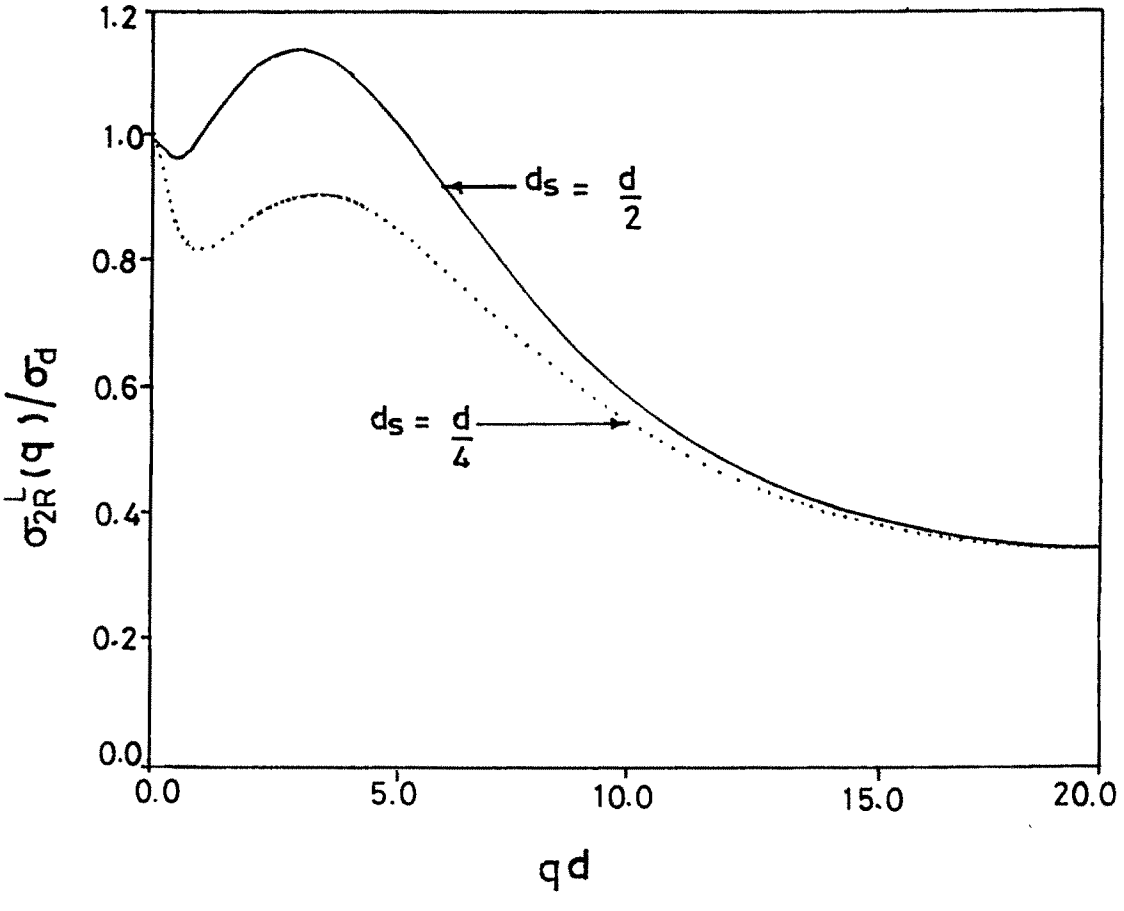

Fig. 4.3 The $\sigma^L_{2R}(\mathbf{q})/\sigma_d$ for DHS is plotted as a function of **q**d for d_s=d/2 (solid line) and d_s=d/4 (dotted curve) at ω=0 and q_zd=0.

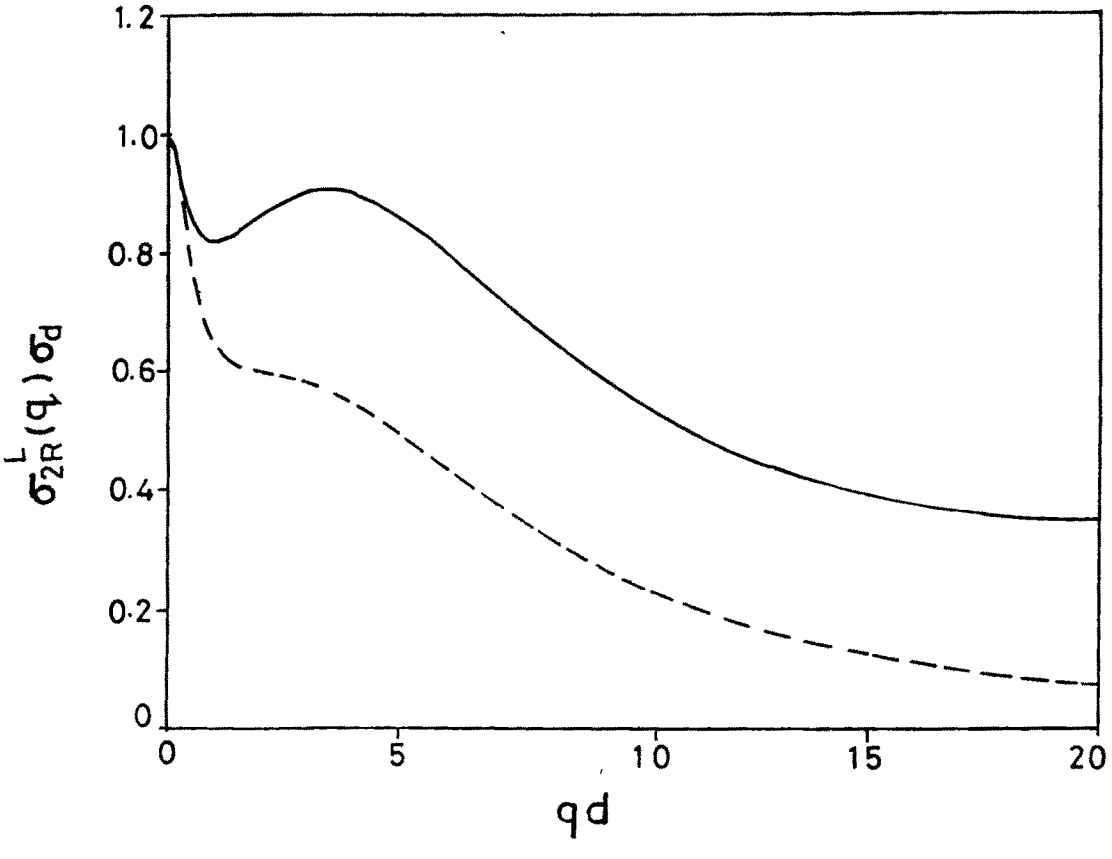

Fig. 4.4(a) The $\sigma^{L}_{2R}(\mathbf{q})/\sigma_d$ for CSSL (dash-dash curve) and DSSL (solid line curve) is plotted as a function of **q**d for ω=0 and $q_z d$=0.

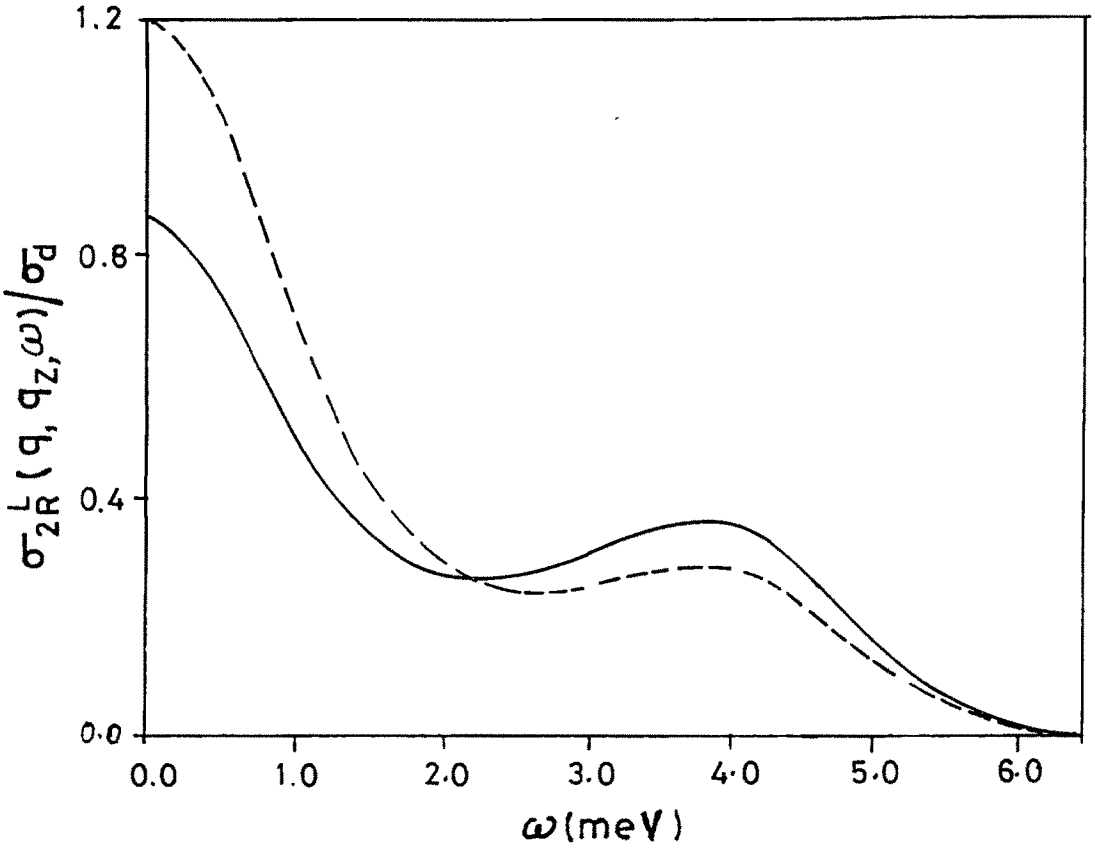

Fig. 4.4(b) The $\sigma^{L}_{2R}(\mathbf{q})/\sigma_d$ for CSSL(dashed curve) and DSSL (solid line curve) is plotted as a function of ω at $\mathbf{q}d=1.0$ and $q_zd=1.0$.

structure. For large value of d ($d\rightarrow\infty$), unit cells become decoupled and DSSL reduces to DHS. The change in d causes a change in Coulomb interaction because of change in layering effect and effective dimensionality. As can be seen from the Fig.4.2(b), $\sigma_{DSSL}<\sigma_{DHS}$ when ω is close to zero and $\omega>qv_{F1}$, whereas $\sigma_{DSSL}>\sigma_{DHS}$ for ω close to qv_{F1}. The macroscopic conductivity of DHS is larger than that of DSSL for $qd<2$, whereas for $qd>2$, $\sigma_{DSSL}>\sigma_{DHS}$. Difference in σ_{DSSL} and σ_{DHS} over different $\mathbf{q}$ and ω regimes is caused by change in Coulomb interaction with $\mathbf{q}$ and ω. Coulomb interaction in DHS is weaker as compared to DSSL for small $\mathbf{q}$ values.

In order to see how separation between two layers in a unit cell affects the conductivity, we computed $\sigma^{L}_{2R}(\mathbf{q})$ for different value of d. Figure 4.3 shows a plot of $\sigma^{L}_{2R}(\mathbf{q})/\sigma_d$ versus qd for two values of d_s (d/2 and d/4) at $q_zd=0$ and $\omega=0$ in GaAs DSSL. As is seen from figure, $\sigma^{L}_{2R}(\mathbf{q})$ is largest for $d_s=d/2$ at all $\mathbf{q}$-values. However, effect of change in d_s reduces on increasing $\mathbf{q}$, and for very large value of qd, $\sigma^{L}_{2R}(\mathbf{q})$ is almost independent of change in d_s. The effect of change in d_s on σ^{L}_{2R} is similar in both DSSL and CSSL2.

We have computed $\sigma^{L}_{2R}(\mathbf{q},q_z,\omega)$ as a function of ω for $qd=1.0$ and $q_zd=1.0$, then as a function of qd at $\omega=0$ and $q_zd=0$ taking same values of m_1, m_2, n_{s1} and n_{s2} for both CSSL2 and DSSL. However, for DSSL used $\varepsilon_{11}=\varepsilon_{22}=10.9$ and for CSSL2 $\varepsilon_{11}=12.4$ and $\varepsilon_{22}=14.4$, in order to see the effect of inhomogeneity in dielectric background on $\sigma^{L}_{2R}(\mathbf{q},q_z,\omega)$. Our computed $\sigma^{L}_{2R}(\mathbf{q},q_z,\omega)/\sigma_d$ is plotted as a function of ω in Fig.4.4(b) and as a function of qd in Fig. 4.4(a). The $\sigma^{L}_{2R}(\mathbf{q},q_z,\omega)/\sigma_d$ of DSSL, which offers same background for electrons and holes, is larger than that of CSSL2, where background of electrons is different than that of holes, at all $\mathbf{q}$-values when $q_zd=0$ and $\omega=0$, as is seen in Fig. 4.4(a). However, $\sigma^{L}_{2R}(\mathbf{q},q_z,\omega/\sigma_d$ of CSSL2 is larger than that of DSSL for ω close to qv_{F1} for fixed qd and q_zd as is seen in Fig.4.4(b). The difference between $\sigma^{L}_{2R}(\mathbf{q},q_z,\omega)$ of DSSL and CSSL2 significant and it is almost same for all $\mathbf{q}$-values. This suggests that the difference in dielectric background of a hole layer and of a electron layer significantly affect the macroscopic conductivity.

4.32 Microscopic conductivity

The microscopic conductivity of system having two layers of charge carriers is given by Eqs.(4.29) and (4.30), where the effects of screening are incorporated in $\varepsilon_2(\mathbf{q},q_z,\omega)$. Solution of $\varepsilon_2(\mathbf{q},q_z,\omega)=0$ for ω as a function of $\mathbf{q}$ and q_zd gives frequency of longitudinal collective excitation modes (plasma oscillations). Propagation of plasma oscillations (with

and without retardation effects) in several types of CSSL2, DSSL and DHS have been discussed by several authors for different wave vector regimes [20-26,50,51]. In view of this, we here discuss only the propagation of TE modes whose frequencies are given by zeroes of $F_2(\mathbf{q},q_z,\omega)$. $F_2(\mathbf{q},q_z,\omega)$ consists of structure factors $U_{ij}(\mathbf{p},q_z)$, which involves $W_{ij}(\mathbf{p},q_z)$. Therefore, $U_{ij}(\mathbf{p},q_z)$ for the case of $\omega/c>\mathbf{q}$ involves $\sin(\mathbf{pd})$ and $\cos(\mathbf{pd})$, which are sinusoidal function. For a given value of $\mathbf{q}$ and q_z, $F_2(\mathbf{q},q_z,\omega)=0$ can therefore be satisfied for more than one value of ω. This suggests that there can exist several TE mode, for one value of $\mathbf{q}d$ and q_zd, in a DSSL, CSSL2 and DHS. Solution of $F_2(\mathbf{q},q_z,\omega)=0$ for ω as a function of $\mathbf{q}$ for $-1\leq\cos(q_zd)\leq1$ provides several bands of frequency of TE modes.

We have computed $\omega_{2t}(\mathbf{q},q_z)$, real part of ω for which $F_2(\mathbf{q},q_z,\omega)=0$, for two lowest bands of TE modes which are linked with each other via interlayer interactions. Our results are plotted in Fig.4.5 for InAs/GaSb CSSL2 whose parameters are as follows: $m_1=0.026\ m_e$, $m_2=0.3\ m_e$, $n_{s1}=n_{s2}=0.7\times10^{12}$ cm^{-2}, $\varepsilon_{1\infty}=12.4$, $\varepsilon_{2\infty}=14.4$, $d_1=650$ Å, $d_2=650$ Å and $\gamma_1=\gamma_2=1.0$ meV. Similar to the case of plasmons (TM modes) in CSSL2 [51], there exist adjoining two bands of TE modes, linked through interlayer interactions and one of the two bands is narrow. Further, like the case of plasmons, lower and upper edge of broad TE mode occur at $\cos(q_zd)=1$ and $\cos(q_zd)=-1$, whereas that of narrow band appear at $\cos(q_zd)=-1$ and $\cos(q_zd)=1$, respectively. However, unlike the case of plasmons; (i) the narrow band appears above the broad band and (ii) frequency of none of TE modes goes to zero as $\mathbf{q}d$ tends to zero, in a CSSL2. As can be seen from figure, $\omega_{2t}(\mathbf{q},q_z)$ is almost proportional to $\mathbf{q}$ for $\mathbf{q}d>1$ at all values of $\cos(q_zd)$. The approximate values of $\omega_{2t}(\mathbf{q},q_z)$ for $\mathbf{q}\rightarrow0$ are obtained by making an expansion of $F_2(\mathbf{q},q_z,\omega)$. For $\mathbf{q}d<<1$ and $\mathbf{p}d<<1$, $H_{ii}(\mathbf{p})\cong C_{ij}(\mathbf{p})\cong H_{ii}(\mathbf{q})\cong C_{ij}(\mathbf{q})\cong1$, where

$$W_{ii}(\mathbf{p},q_z)\cong\mathbf{p}d/[1-\cos(q_zd)+(\mathbf{p}d)^2/2] \qquad (4.43)$$

and

$$W_{ii}^2(\mathbf{p},q_z)-W_{ij}(\mathbf{p},q_z)W_{ji}(\mathbf{p},q_z)\cong(\mathbf{p}d)^2/[2-2\cos(q_zd)+(\mathbf{p}d)^2]. \qquad (4.44)$$

The $W_{ii}(\mathbf{q},q_z)$ and $W_{ij}(\mathbf{q},q_z)$ are obtained from Eqs.(4.43) and (4.44) on replacing $\mathbf{p}$ by $\mathbf{q}$. Solution of $F_2(\mathbf{q},q_z,\omega)=0$ with the use of $U_{ij}(\mathbf{p},q_z)$ and $U_{ij}(\mathbf{q},q_z)$, calculated using Eqs.(4.43) and (4.44), yields

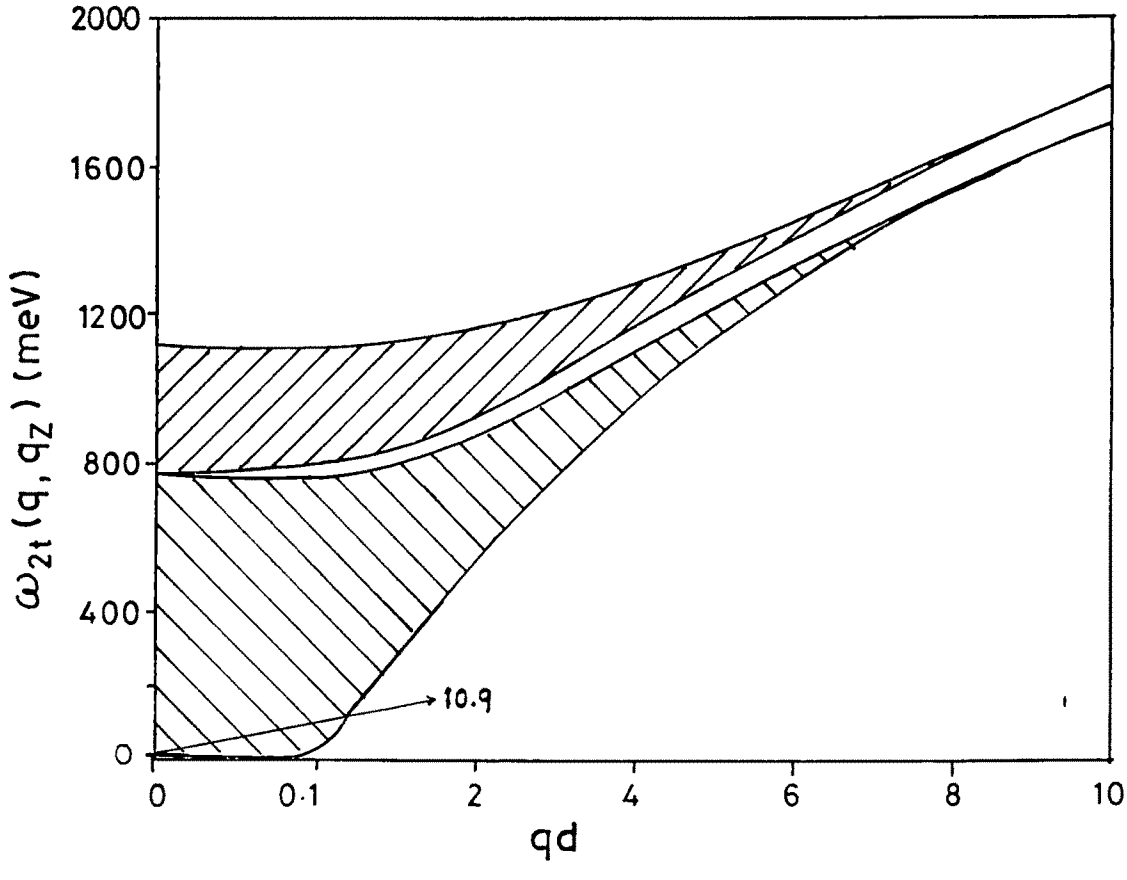

Fig. 4.5 A plot of $\omega_{2t}(\mathbf{q},q_z)$ as a function of $\mathbf{q}$ for $-1 \leq \cos(q_z d) \leq 1$.

$$\omega^2_{2t}(\mathbf{q},q_z) = [-B \pm (B^2-4AC)^{1/2}] / 2A, \qquad (4.45)$$

where A, B and C are defined as

$$A = (d^4/4c^4)\,[\varepsilon_{11}\varepsilon_{22}-\varepsilon_{11}-\varepsilon_{22}+1], \qquad (4.46)$$

$$B = (d^4/4c^4)\,[\alpha+\beta-\varepsilon_{22}\alpha-\varepsilon_{11}\beta] - (d^2/4c^2)\,[\varepsilon_{22}+\varepsilon_{11}-1], \qquad (4.47)$$

$$C = 2-2\cos(q_z d)+(qd)^2+(d^2/4c^2)(\alpha+\beta)+(d^4/4c^4)\alpha\beta \qquad (4.48)$$

with

$$\alpha = (4\pi n_{s1}e^2/m_1 d)\,(qd)^2 / [2-2\cos(q_z d)+(qd)^2] \qquad (4.49)$$

and

$$\beta = (4\pi n_{s2}e^2/m_2 d)\,(qd)^2 / [2-2\cos(q_z d)+(qd)^2]. \qquad (4.50)$$

Equation (4.45) with plus sign on right hand side gives upper band and it gives lower band of Fig 4 5 when there is negative sign on right hand side.

The characteristics of TE modes for real and imaginary wave vector values, which have been discussed in chapter III for the case of type-I superlattices, have also been observed for DSSL, CSSL2 and DHS. On making comparative study of TE modes in type-I and type-II superlattices for real and imaginary value of $\mathbf{q}$ and q_z, we have not find any new thing to be reported in this chapter.

4.4 Conclusion

We have computed $\sigma_2^{L/T}(\mathbf{q},q_z,\omega)$ and $\tilde{\sigma}_2^{L/T}(\mathbf{q},q_z,\omega)$ for DSSL, CSSL2 and DHS. The $\sigma_2^{L/T}(\mathbf{q},q_z,\omega)$ is the sum of $\sigma'_{L/T}(\mathbf{q},q_z,\omega)$ and $\sigma''_{L/T}(\mathbf{q},q_z,\omega)$. $\sigma'_{L/T}(\mathbf{q},q_z,\omega)$ contribute to $\sigma^{L/T}(\mathbf{q},q_z,\omega)$ for all values of $\mathbf{q}$ and q_z, while $\sigma''_{L/T}(\mathbf{q},q_z,\omega)$ contribute only when $\mathbf{q}\neq 0$. Unlike the case of $\sigma_{2R}^{L}(\mathbf{q},q_z,\omega)$, interlayer interactions do not contribute significantly to $\sigma_{2R}^{T}(\mathbf{q},q_z,\omega)$ and for $\omega\rightarrow 0$ contribution from interlayer interactions is zero. In DSSL, CSSL2 and DHS interlayer interactions play an important role in determining peak positions and

peak heights. The shape of the peak, position and behaviour of the peak is also governed by n_{s1}, n_{s2}, m_1, m_2 and d in DSSL, CSSL2 and DHS The broad feature of the two peaks in $\sigma^{L}_{2R}(\mathbf{q},q_Z,\omega)$, which correspond to single particle excitations are similar to that of single particle excitation peak in $\sigma_R(\mathbf{q},q_Z,\omega)$ reported in chapter III. It is found that for $d\rightarrow\infty$, unit cells of DSSL become almost decoupled and DSSL reduces to DHS. Change in d causes a change Coulomb interaction because of change in layering effect and effective dimensionality. Therefore, difference in σ_{DHS} and σ_{DSSL} over different ω and $\mathbf{q}$ regimes is caused by the change in Coulomb interaction with $\mathbf{q}$ and ω. $\sigma^{L}_{2R}(\mathbf{q},q_Z,\omega)$ is largest for $d_s=d/2$ at all $\mathbf{q}$-values and the effect of change in d_s reduces on increasing $\mathbf{q}$ in a DSSL. The $\sigma^{L}_{2R}(\mathbf{q},q_Z,\omega)$ of DSSL, which offers same background for electrons and holes, is larger than that of CSSL2, where background of electrons is different from that of holes at all $\mathbf{q}$-values, where same value of n_{s1}, n_{s2}, m_1 and m_2 is taken for both DSSL and CSSL2. This suggests that the difference in dielectric background of electron and hole layer significantly affect the macroscopic conductivity. The propagation of TE modes where frequencies are given by zeroes of $F_2(\mathbf{q},q_Z,\omega)$ has been discussed. Solution of $F_2(\mathbf{q},q_Z,\omega)=0$ for ω as a function of $\mathbf{q}$ for $-1\leq\cos(q_Zd)\leq1$ provides several bands of frequency of TE modes. Two adjoining lowest bands of TE modes are found to be similar to those of plasmons (TM modes) in CSSL2. Unlike the case of plasmons, narrow band appears above the broad band and frequency of none of TE mode goes to zero as $\mathbf{q}d\rightarrow0$

REFERENCES

[1] G. Bastard, Phys. Rev. B 24, 4714 (1981).[2] "The technology and physics of molecular beam epitaxy", edited by E.H.C. Parker, (Plenum Press, New York and London, 1985).

[3] G.H. Dohler, Phys. Status Solidi.(b) 53, 79 (1972); Phys. Status Solidi.(b) 52, 533 (1972), Surf. Sci. 73, 97 (1978).

[4] G.H. Dohler, Proc. Conf. on the Phys. And Tech. of semiconductor device and integrated circuits (Proc. SPIE 1523 Bellingham, WA: SPIE) pp. 22-63.

[5] R.Ruden and G.H. Dohler, Phys. Rev. B 27, 3538 (1983).

[6] G.F. Giuliani and J.J. Quinn, Phys. Rev. B 29, 2321 (1983).

[7] C. Metzner, H.J. Beyer and G.H. Dohler, Phys. Rev. B 46, 4128 (1992).

[8] T. Ando, T.B. Fowler and T.F Stern, Rev. Mod. Phys. 43, 437 (1982).

[9] A. Sai Halasz, L.L. Chang, J.M Welter, C.A. Chang and L.Esaki, Solid State Commun. 27, 935 (1978).

[10] F. Minami, K. Hirata, K. Era, T. Yao and Y. Masumota, Phys. Rev. B 36, 2875 (1987).

[11] D. Redfield, Adv. Phys. 29, 463 (1995).

[12] P. Voisin, G. Bastard et. al. Solid State Commun., 39, 729 (1981)

[13] H. Kunzel, G.H. Dohler, P. Rudes and K. Ploog, Appl. Phys. Lett. 41, 852 (1982).

[14] W. Sritrakool, V. Sa-ya Kanit, H.R. Glyde, Phys. Rev B 32, 1090 (1985).

[15] G.B. Boos, W. Kruppa, B.V. Shanabrook, D. Park, J.L. Davis and H.B. Dietuch, Elec. Lett. 29, 1888 (1993).

[16] W. Langbein and H. Kall, Phys. Rev. B 54, 14589 (1998).

[17] F. Betran and F. Cappsse, Phys. Rev. B 38, 3580 (1988).

[18] Y.A. Puxp, A.J. Chiquiro, S. Mergubhas, J.C. Gatzerane, Phys. Rev. B 56, 3892 (1997).

[19] T. Anand, J Bareu, X. Marie, N. Laurel . B. Dareys, M. Brousseum, F. Laruella, Phys. Rev. B 47, 7155 (1993).

[20] S. Das Sarma and J.J. Quinn, Phys. Rev. B 25, 7603 (1982).

[21] A.C. Tselis and J.J. Quinn, Phys. Rev. B 29, 2021 (1984); Phys. Rev. B 29, 3318 (1984).

[22] N. Tzoar and C Zhang. Phys. Rev. B 34, 1050. (1986)

[23] P. Hawrylak, G. Eliasson and J.J. Quinn, Phys. Rev. B 34, 5368 (1986).

[24] S. Whankim and K.S. Sohn. Phys. Rev. B 50. 17185 (1994)

[25] R.E. Camely and D.L Mills, Phys. Rev. B 29. 1695 (1984).

[26] W. Liu, G. Eliasson and J.J. Quinn, Solid State Commun. 55, 5333 (1985).

[27] J.S. Nikoma, Surf. Sci. 191. 595 (1987).

[28] S.R. Streight and D.L. Mills, Phys. Rev. B 35. 6337 (1978).

[29] B.L. Johnson. J T. Weiler and R.E. Camely, Phys. Rev. B 32, 6544 (1985)

[30] N. Mori and T.Ando. Phys. Rev. B 40. 6175 (1989).

[31] T.T. Suchiya and T. Ando. Phys. Rev B 47, 7240 (1993).

[32] R. Tsu and S S. Jha, Appl. Phys Lett. 20, 16 (1972).

[33] B. Vinter, Phys Rev Lett. 45, 581 (1984).

[34] B.K. Ridley, Phys. Rev. B 39, 5282 (1989).

[35] P. Castmillo, L. Colombo and G. Armelles, Phys. Rev. B 49, 10362 (1994).

[36] N. Sawaki, J. Phys. C 19, 4965 (1986).

[37] N. Tzoar and C. Zhang, Phys. Rev. B 33, 2642 (1986); Phys. Rev. B 32, 1146 (1985).

[38] X.L. Lei, H.L. Cui and N.J.M. Horing, Phys. Rev. B 32, 1112 (1985).

[39] X.L. Lei, Phys. Rev. B 32, 1119 (1986).

[40] X.L. Lei, H.L. Cui and N.J.M. Horing, Phys. Rev. B 38, 8230 (1988).

[41] D.L. Smith and C. Mailhiot, J. Appl. Phys. 62. 2545 (1987).

[42] C.R. Bologneri. H. Kromer and J.H. English, Appl. Phys. Lett. 61, 213 (1992).

[43] J.F. Palmier and A. Chomette, J. Phys. 43. 381 (1982).

[44] J.R. Mayer, D.J. Arnold, C.A. Hoffmann and F.J. Bardoli, Phys. Rev. B 45. 1295 (1992).

[45] E.E. Mendez, G. Bastard, L L. Chang, C.A Chang and L. Esaki, Bull. Am. Phys. Soc. 29, 471 (1984).

[46] A. Sibille, J.F. Palmier, F. Mullot, H. Wang and J.C. Esnaut, Phys. Rev. B 39, 6272 (1989).

[47] F. Betran, F. Copasso, D L. Sovco, A.L. Hulchinson, S.G. Chen and A.Y. Cho, Phys. Rev Lett. 64. 3167 (1990).

[48] C.A. Hoffmann, J.R. Meyer, F.J. Bartoli and W L. Wang, Phys. Rev. B 48. 1959 (1993).

[49] A.C. Sharma and A.K. Sood, J Phys.: Condens. Matter 6. 1553 (1994)

[50] A.C. Sharma and R. Sen, J. Phys.: Condens. Matter 7, 9551 (1995).

[51] A.C. Sharma, R. Sen and P.Tripathi, J. Phys.: Condens. Matt. 9, 8041 (1997).